IEEE Access
Multidisciplinary | Rapid Review | Open Access Journal

Received February 20, 2019, accepted March 3, 2019, date of publication March 21, 2019, date of current version April 10, 2019.

Digital Object Identifier 10.1109/ACCESS.2019.2906566

Breast Phantom Imaging Using Iteratively Corrected Coherence Factor Delay and Sum

SALEHIN KIBRIA, MD SAMSUZZAMAN, (Member, IEEE), MD TARIKUL ISLAM, MD ZULFIKER MAHMUD, NORBAHIAH MISRAN, AND MOHAMMAD TARIQUL ISLAM, (Senior Member, IEEE)

Center of Advanced Electronic and Communication Engineering, Universiti Kebangsaan Malaysia, Bangi 43600, Malaysia

Corresponding authors: Salehin Kibria (kibriasalehin@gmail.com), Md Samsuzzaman (samsuzzaman@ukm.edu.my), and Mohammad Tariqul Islam (tariqul@ukm.edu.my)

This work was supported by the University Research Grant under Project MI-2018-016.

ABSTRACT In this paper, a system for microwave breast tumor detection is presented using iteratively corrected coherence factor delay and sum (CF-DAS) algorithm. CF-DAS is data independent, which makes it stable in a noisy environment. However, data adaptive techniques have made significant progress by enhancing the image quality in microwave tomography. Thus, a novel data adaptive iterative variant of CF-DAS is proposed in this paper to produce stable and accurate images. The microwave imaging (MI) system contains a rotatable array of nine modified antipodal Vivaldi antennas in a circular arrangement, an array-mounting stand based on the stepper motor, the flexible phantom mounting podium, a control system for RF switching of the transceivers, and signal processing unit based on personal computer involved in the reconstruction of the image. The impedance bandwidth of the modified antenna is recorded from 2.5 to 11 GHz with stable directional radiation pattern. For performing the transmission and reception of the microwave signals, an SP8T nine port RF switch is used ranging from 2.5 to 8.0 GHz, and the switching is controlled by MATLAB software. Several low-cost lab-based homogenous and heterogeneous phantoms containing the dielectric property of human breast and tumor tissue are prepared to test the system efficiency. Since typical data independent radar-based techniques are ill-equipped for multiple reflection scenarios, an iteratively corrected variant of CF-DAS algorithm is used for processing the recorded backscattered signals to reconstruct the image of the breast phantom and to identify the existence and locate the area of the multiple breast tumors. The proposed method achieves more than 10-dB improvement over conventional CF-DAS in terms of signal to mean ratio for four different phantoms measured in this study.

INDEX TERMS Breast phantom, CF-DAS algorithm, tumor detection, antipodal Vivaldi antenna array, microwave imaging.

I. INTRODUCTION

More than 2 million new breasts cancer cases are diagnosed each year worldwide [1]. X-ray mammography, Computed Tomography (CT), Ultra-Audio (US), Magnetic Resonance Imaging (MRI) are generally used as diagnostic equipment for identifying breast cancers [2], [3]. Nevertheless, X-ray mammography utilizes ionizing radiation, requires unpleasant compression of the breasts during the examination. Additionally, the ionization initiated by X-ray mammography has several side effects, which paradoxically contains the probability of turning healthy cells malignant.

The associate editor coordinating the review of this manuscript and approving it for publication was Raghvendra Kumar Chaudhary.

Additionally, the deep-lying cancerous cells are hard to detect. Magnetic Resonance Imaging (MRI) gives high-resolution pictures. However, the price is very high [4]. Therefore, microwave imaging is now a promising method for breast tumor detection because of non-ionizing radiation effect.

Microwave imaging (MI) is a technique that maps the distribution of electrical property in objects. The contrast between the dielectric properties of normal and tumorous tissue is the fundamental of microwave imaging. The microwave antennas can easily distinguish the small signal fluctuations from the variations of the electrical properties of human tissues. However, interpreting those variations

into accurate reconstructions of the internal structure is a challenging task as it is an ill-posed inverse scattering problem. Single or several antennas receive scattered and radiated power in MI. The water and other organic contents of every biological tissue vary causing different electrical properties [5]. A variation in the dielectric property of the material is experienced by microwave while traveling through abnormal tumorous tissue that results in scattering of the incident wave. This scattering energy is detected at the receivers. The information of detected energies is utilized to form the imaging result.

Various categories of antennas are proposed and used for phantom breast measurements, for instance, Pyramidal Horn Antenna [6], Vivaldi antenna [7]–[10], CPW antenna [11], metamaterials and EBG antenna [12], [13], and the slotted antenna [9], [14]–[16]. For the development of an effective MI system with dynamic range and high resolution, the antenna utilized for transmitting and receiving should be wideband, compact, directive and high radiation efficiency. The wideband characteristics provide high resolution and accurate localization of a target for imaging. Besides, in a single test, information over a wide frequency band can be collected and leading to the feasibility of fast data acquisition and rapid microwave detection. In a near field wideband detection, only a single or small number of low microwave energy pulse needed which is an important requirement for electromagnetic medical applications [6]. In this scenario, the Vivaldi antenna is a suitable contender for its highly directional radiation beam, compact dimensions, and high gain. The primary design challenge of an antipodal Vivaldi antenna is to get directional radiation pattern and lower frequency impedance bandwidth with compact dimensions. Last few years, Vivaldi antenna design has received much attention for medical applications due to its desirable properties [17]. To enhance the performance of the Vivaldi antenna, several studies have introduced different methods [7]–[10], [17]. However, a compact antenna with improved antenna property like broad impedance and the high gain antenna was desired for microwave imaging applications.

Numerous simulation and experimental microwave imaging system results have been reported regarding breast tumor detection [11], [16], [18]–[23]. Microwave system containing 16 wideband antennas was presented to monitor the dielectric variation of breast tissue [11], [16], [21], [22]. The time domain signal was gathered by an oscilloscope and antenna from 2-4 GHz frequency range. 20 monopole antennas were utilized in a lossy medium time domain system for medical applications through the UWB frequency range (100 MHz to 3 GHz) [24], [25]. In [23], 16 UWB antennas were used on the side of the phantom. To switch the antenna, a master controller was positioned at the top of the array. So far discussed in the imaging mentioned above system, most of the designed system was used many antennas to received multiple signals with adjustable low coupling antenna elements in the limited space. To solve the switching complexity of channel, to mitigate the antenna couplings and to develop the cost-effective system, the dynamically movable antenna would be utilized to collect the backscattered signal in multiple locations is a better alternative solution instead of the fixed antenna array. Based on the rotation angle, the movable antenna array is able to collect data for multiple illumination angles. Initially, a biostatic antenna system was used for transceiver and receiver with a fixed rotating arc to collect the equal number of signals for processing as like monostatic system [26]. Later multi-static imaging system was introduced to collect more signal for high-resolution image construction [27], [28]. A 4×4 planar UWB antenna array was proposed for 3D breast cancer detection, but the study used only the simulation setup to identify the tumor [29]. A monostatic system in which a balanced antipodal antenna was used to collect the backscattered signal from 36 six different positions around the object [8]. Another study proposed a 16 fixed antipodal Vivaldi antenna with a rotatable head phantom object for head imaging applications [9]. Artificial Magnetic Conductor (AMC) inspired CPW fed antenna based microwave imaging was developed into a two rotating antenna array system for detecting the commercially developed phantom with single tumor object [3]. To sequentially send microwave signal to head phantom, a switch matrix was used to enable the antennas to receive backscattered signal although the author has performed the pilot clinical test through the system. Two big sizes UWB band antenna was proposed with a rotatable platform where the antennas can collect 24×19 transmission and reception data within 10 minutes [6]. Recently, a 16 cross-shaped antenna array was applied to design a portable microwave imaging system for breast tumor detection where design system comparatively complex in structure and difficult to distinguish the tumor presence [30], even though the author has investigated small-scale clinical study to detect the tumor with the designed system. Availability of such a system is essential to test various methods and techniques that might help to make a complete preclinical breast imaging system.

Data independent inverse scattering techniques like DAS are popular due to the simplicity of implementation and stable results. Several data independent variants of DAS like DMAS [3], [6], [9]–[11], [13], [16], [23] CF-DAS and several others have been proposed to improve the performance of DAS. DAS and its variants rely on the coherent summation of appropriately delayed signals to determine the size and brightness of the scattering objects present. The delays are calculated based on the time required for electromagnetic waves to travel the total distance from transmitting antenna to the point of interest and back to the receiving antenna. Various other data independent algorithms are used for microwave imaging like TSAR (Tissue Sensing Adaptive Radar) [8], Confocal Imaging [29]. However, DAS and its variants are significantly more popular due to their simplicity and robust performance. The scattering phenomenon occurs at boundaries of materials with different dielectric properties in a heterogeneous environment. The heterogeneity of the typical imaging targets changes the travel time of electromagnetic

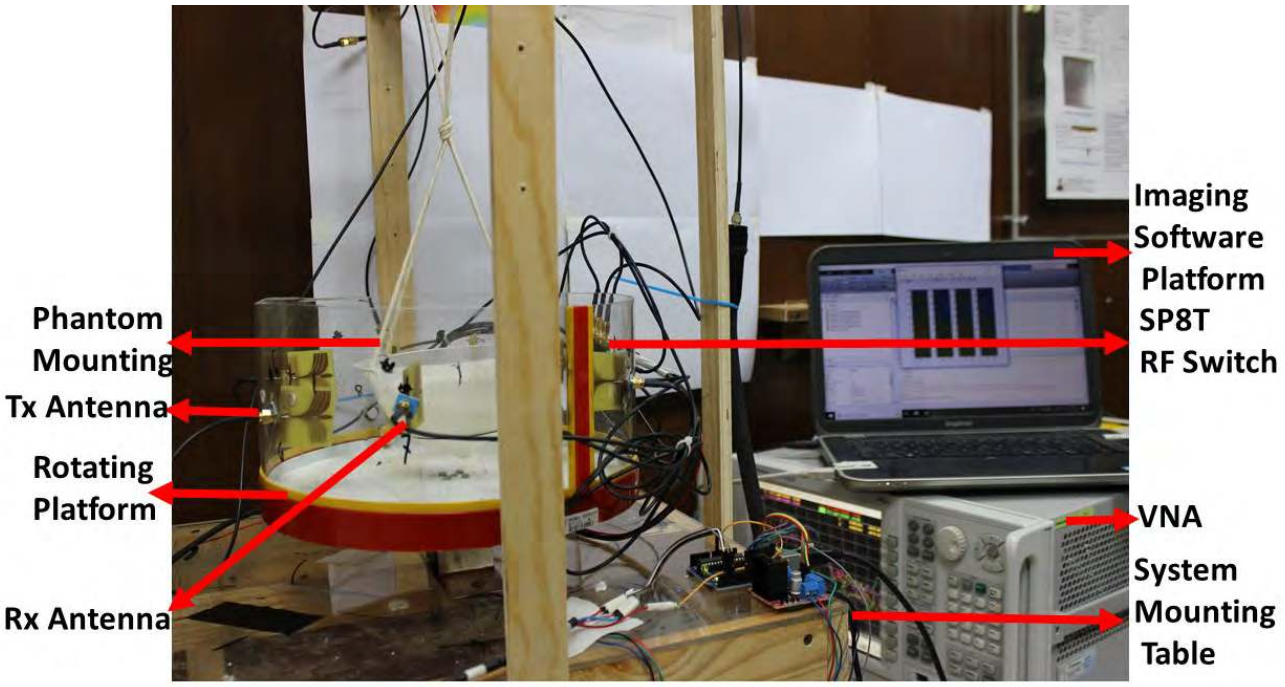

FIGURE 1. The architecture of the proposed imaging system experimental setup.

waves, which is critical for DAS based algorithms. This is an inherent drawback to data independent techniques, as they possess no mechanism to account for such delay variations due to phantom inhomogeneity. Furthermore, DAS is prone to 'ghosting' due to multiple reflections produced in the presence of multiple scattering anomalies typically present in human breasts. Born approximation [31], [32] is used to detect weak scattering objects that do not alter the incident field significantly. It assumes that the scattered field is produced by the linear summation of all the echoes produced by dielectric inhomogeneities in the region concerned. However, Born approximation fails in the case of complex structures with many scattering interfaces as multiple reflections are not considered. Thus, the modified technique based on Born approximation was presented in literature named Distorted Born Iterative Method (DBIM) to robustly adapt to the reconstructed image and iteratively improve the result to fit the measured scattering field. Data adaptive tomographic approaches like DBIM are superior to independent data techniques as they generate more detailed information about the dielectric properties of the phantom under investigation [33], [34]. However, these data adaptive techniques can often become unstable and diverge, especially in high noise environments.

In this research article, we have presented the design and development of an imaging system using a DBIM inspired radar-based technique with an iteratively adjusted time delay to improve imaging performance. The developed imaging system can be utilized to detect the tumor and its position in case of breast imaging. In this system, a nine improved antipodal Vivaldi antenna array with wideband coverage is implemented to send and receive signals. Radiating fins and parasitic ellipse was used to enhance the impedance matching and directionality performance of each antipodal Vivaldi antennas. Several lab-made breast phantoms have also been fabricated and measured using a dielectric coaxial probe kit. The MATLAB based software and imaging system hardware complete the data collection procedure within three minutes for 8×50 scanned channels, as illustrated in Section II. After processing the collected microwave backscattered data, reconstructed image results had been acquired to detect the high dielectric multiple tumor objects embedded in the phantoms presented in Section III by using the iteratively enhanced coherence factor delay and sum algorithm presented in Section IV. Finally, the results of the imaging system are presented and briefly discussed in Section V, followed by concluding remarks in Section VI.

II. COMPONENTS OF THE IMAGING SYSTEM

An imaging system experimental setup to check the feasibility of using microwaves for breast tumor detection is demonstrated in Figure 1.

The designed breast imaging system operates across the 2.5 to 8 GHz frequency band. The imaging system antenna includes an improved parasitic ellipse, and balanced slot loaded antipodal Vivaldi antenna array of nine elements that are installed with rotatable circular plastic container platform, SP8T RF switch, lab-based phantom, stepper motor, microcontroller, vector network analyzer and data capturing unit with a PC. The details of each of the below experimental setup have explained in the following sections.

A. ANTENNA DESIGN STRUCTURE AND ARRAY DESIGN

The primary purpose of this antenna design is to categorize the variance in dielectric properties between malignant (tumor object) and the healthy breast tissue. For considerably better penetration and high-resolution imaging, multiple resonance frequencies are necessary at the cavernous part of the breast [35]. High gain, lower resonant frequency, and directive radiation antenna properties are desirable for microwave imaging. The proposed antenna was derived from our previous version antipodal antenna [10]. The geometric design and fabricated prototype can be found in Figure 2 where FR4 is used as the substrate material with 1.6 mm thickness, the relative permittivity of 4.4 and loss tangent of 0.02. In this antenna design, FR4 used as substrate material due to lower manufacturing cost, ease of fabrication, design flexibility and market availability of the proposed material compare to other material. Nowadays it has become popular in the research and industry community for use as a substrate in patch antenna design although it's lossy property to high frequency. The antenna covers the dimension of $40 \times 40 \times 1.6\text{mm}^3$ with modified patch and ground, an elliptical notch for increasing the directivity of the radiating elements and a 50-Ω microstrip feed line. Asymmetrical slots and elliptical expansion are analyzed for increasing the electrical length to improve lower band performance. These fine cuts and elliptical extension at patch have a substantial effect on surface current distribution that leads to achieving the lesser resonance and directive gain. The optimized design parameters are as follows: $L = 40mm, g_1 = 1.4mm, W_1 = 35mm, C_1 = 8mm, d_1 = 9mm, r_1 = 6mm, d_2 = 12mm, r_2 = 1.5mm, a = 24mm, h = 1.6mm, d_{3=8mm}$.

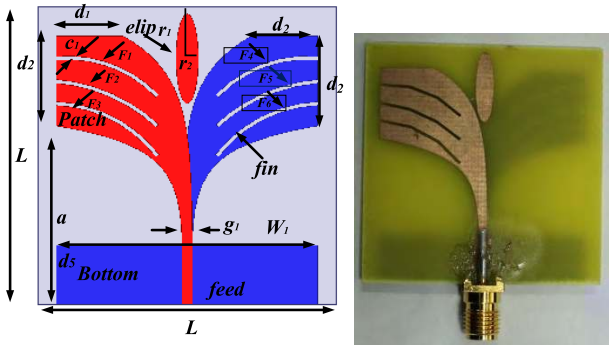

FIGURE 2. (a) Geometric layout and (b) fabricated prototype.

B. ANTENNA PERFORMANCE MEASUREMENT

The antenna performance of the proposed prototype has been investigated and optimized by using the CST microwave studio solver. The antennas radiation characteristics are measured from UKM Satimo Star lab. The measured and numerical reflection coefficient (S_{11}) curves of the antenna are presented in Figure 3. The antenna achieves an operating

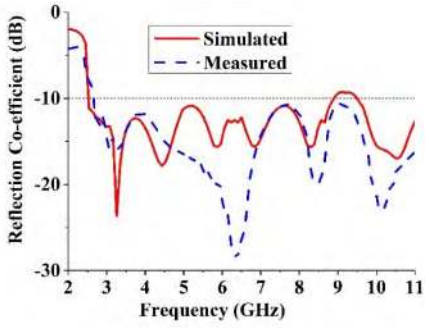

FIGURE 3. The numerical and measured reflection coefficient(S_{11}) of the designed antenna.

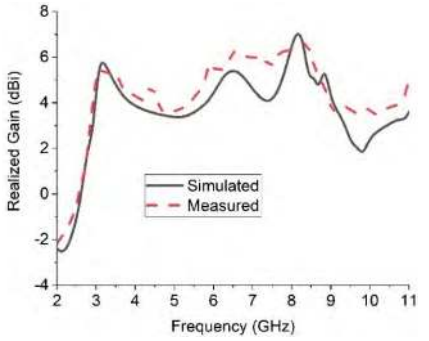

FIGURE 4. The numerical and measured realized gain of the proposed antenna.

bandwidth of above 8.4 GHz (125.92%) ranging from 2.50 to above 11 GHz frequency ranges. The first resonance frequency is shifted to 2.5 GHz, and the highest peak is observed at 6.30 GHz at measurement with numerous peaks across the bandwidth. It can be seen that there are some deviations between the measured and simulated reflections coefficient in the middle frequency, which may be caused by the coaxial cable utilized in the experiment, soldering effect and the fabrication imperfections and the variation of dielectric properties of the FR-4 within tolerance levels. The numerical and measured peak realized gain versus frequency is depicted in Figure 4. The antenna has a higher gain at the lower frequency band and continues to the higher bands that are important for MI systems. The average realized gain is six dBi together with a maximum peak of 7.2 dBi at 8.3 GHz. The antenna achieves an improved gain likened to recently reported antipodal Vivaldi antennas [10]. Radiating fins and parasitic ellipse was used to enhance the impedance matching and directionality performance of each antipodal Vivaldi antennas. The 2D and 3D radiation patterns of measured and simulated experiments are demonstrated in Figure 5 for two different resonance frequencies of 3.25 and 7.0 GHz at XZ-plane ($\phi = 0°$). The realized antenna is directional, and the main radiator directed towards the boresight observed from the far-field measurement. The key lobes of the radiation patterns are fixed towards the end-fire direction over the entire operating band.

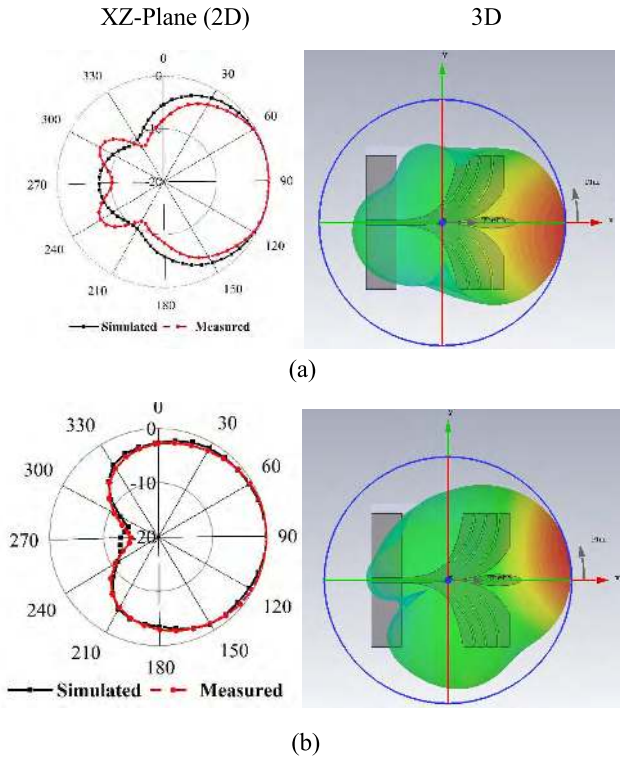

FIGURE 5. 2D, 3D measured and numerical radiation patterns of two frequencies at (a) 3.25 GHz (b) 7.0 GHz.

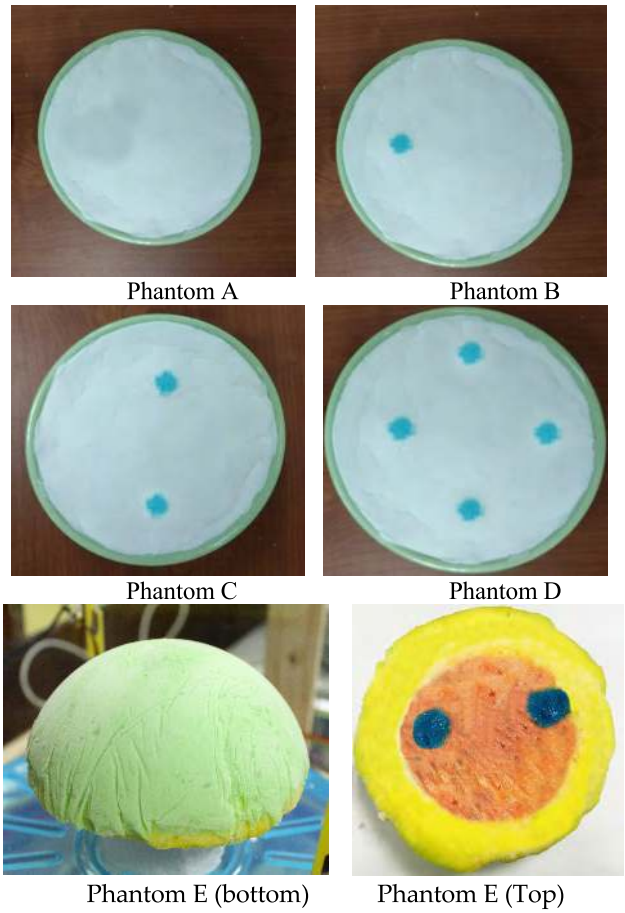

FIGURE 6. Laboratory-based Homogeneous phantoms, without tumor (Phantom A), with a single tumor (Phantom B), with two tumors (Phantom C), with four tumors (Phantom D) and Heterogeneous Phantom (Phantom E).

III. IMAGING PHANTOM DEVELOPMENT AND MEASUREMENT

The breast imaging system is designed to evaluate the imaging performance of detecting breast tumor using a realistic breast phantom. Two types of breast phantom are fabricated and measured according to the methods stated in [36]. The radii of the phantoms are 55 mm (phantoms A, B, and C), and 60 mm (phantom D and E) as displayed in Figure 6. The tumor height and radius are 20 mm and 5 mm, respectively. Phantom A is a homogeneous phantom without any tumors. It serves as the control test that should appear blank due to the rotation subtraction method. Phantom B is constructed by adding a tumor 25 mm away from the center of the structure. This will be the basic test where the imaging system must detect only a single target. Normally, DAS based methods excel in such situations as reflections off only one target must be considered. A more challenging Phantom C is created by replicating phantom B and adding another tumor on the opposite side of the center at an approximately equal distance. The presence of multiple targets can cause multiple internal reflections to misguide the imaging system. Finally, Phantom D is constructed slightly larger at a radius of 60 mm as it is intended for four tumors. The tumors are also placed slightly further apart at 35 mm at 90-degree intervals around the center to maintain the structural integrity of the phantom. Mapping four different targets is usually not attempted or presented in most literature, as it is often difficult for DAS based techniques, which were developed mostly as single target detection methods. Furthermore, a more realistic heterogeneous phantom E with four layers (skin, Fat, Gland, and Tumor) is also presented as phantom E in Figure 6, which has more realistic dielectric properties and 3D construction like a real human breast.

Figure 7 represents the measured and targeted dielectric constant and electrical conductivity of each material of phantoms against frequency. The measurement has been carried out by using the Agilent coaxial probe kit. The dielectric constant and conductivity of homogenous phantom in figure 7 a, b are identical with the targeted curves. Also, the properties of each material (skin, fat, gland and tumor) of Heterogeneous phantom shows in figure 7 c, d proves the accurate measurement properties with the targeted values. Therefore, the results of the phantom properties in this paper have more realistic characteristics of the real human breast to be tested with the microwave imaging system efficiency.

IV. MICROWAVE IMAGING PLATFORM

The breast imaging system is designed to evaluate the imaging performance of detecting breast tumor using a realistic breast phantom. Generally, antennas with very low

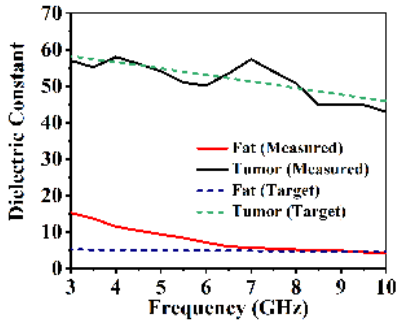

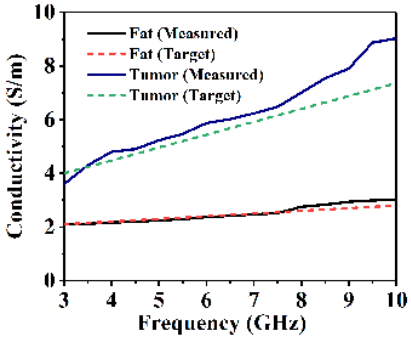

(b)

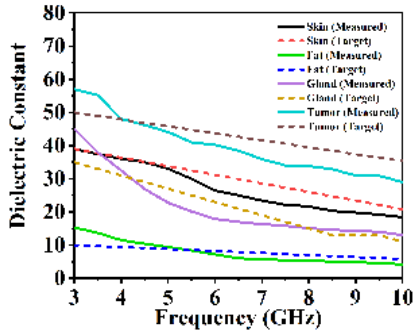

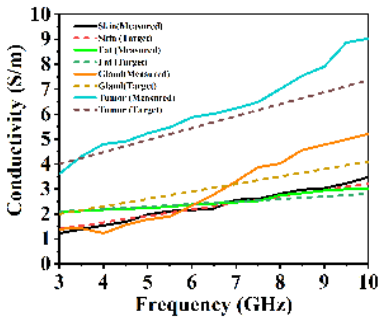

(d)

FIGURE 7. The dielectric constant and electrical conductivity of each material of homogenous (a, b), and heterogeneous phantom (c, d).

return loss are ideal for detecting weak reflected signals. The experimental setup of the breast imaging system is depicted in Figure 1. The used microwave imaging system

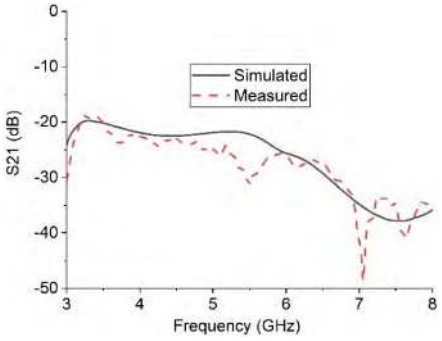

FIGURE 8. Mutual coupling between a pair of adjacent antennas.

comprises of a nine-antenna array, one transmitting(Tx) and eight receiving (Rx) the signals, the stepper motor-based antenna mounting stand, an RF switching system to activate receivers one at a time and the MATLAB based personal computer-based signal processing and image reconstruction unit. The required nine circular array antennas are mounted on a rotating plastic container as illustrated in Figure 1. The diameter of the plastic container is near about 28 cm. The minimal distance between nearby antenna components in the designed array is optimized for less than -20dB of mutual coupling (S_{21}) as portrayed in Figure 8 (simulated and measured). The optimized antenna array space is between 65 mm. The breast phantom is positioned inside the antenna array and scanned using the designed UWB antenna array. The distance between antennas to phantom is near about 30 mm. The turntable platform rotates the antenna array in a complete revolution around the breast phantom using the stepper motor. The antennas are connected to an SP8T (9 Port) non-reflective positive control switching network using low loss coaxial cables. The received signal from all eight receivers is collected by switching the receiving antennas. The data (S21, S31, S41,....S81) are collected in each 7.2°, and $N\varphi = 50$ equally spaced points cover the total 360°. The imaging system uses an Agilent vector network analyzer (VNA) microwave transceiver. The port 1 of VNA generates microwave pulses and transmits it to the breast phantom. The backscattered signal is received by another port via an RF switch and forwarded to the image-processing unit. The collected data are processed by the PC using the proposed algorithm, which reconstructs the image of the breast interior to detect the tumors. The eight distinct channels are calibrated over the operating frequency using a SOLT calibration kit. The antennas are connected to VNA. The VNA parameters are set as 10 dBm output power and no of frequency points N_f is 201 evenly spread out over the operating frequency range of the antenna prototype. The VNA is connected to PC and data are received via a GPIB port for further processing. By using experimental setup, the complex frequency domain S-parameters, S (f, Rx, φ) data are captured, where $Rx = 1, 2 \ldots 8$, is the receiving antenna number, f is the frequency, and φ is the rotational orientation of the platform. A total of 50 × 8 scanned position of data

is collected by using the designed rotated platform within three minutes. The collected data is post-processed using the proposed iterative radar-based algorithm, and the image of the breast interior is reconstructed in the following section.

V. IMAGE RECONSTRUCTION ALGORITHM

Methods to remove the reflections from the skin are critical for detecting scattered signals from inside the phantom since reflection from the air-skin interfaces in orders of magnitude is stronger than the reflections from the tumor tissue. Rotation subtraction relies on a comparison between an original illumination and at least one rotated illumination [37]. In such systems, the antenna array is placed around the region of interest. Once the data is recorded for the original illumination, the array is rotated around the phantom to get offset data. In this study, the $S(f, Rx, \varphi)$ is separated into two matrices on the basis of φ being odd and even, or $S_{odd}(f, Rx, \varphi_{odd})$ and $S_{even}(f, Rx, \varphi_{even})$, respectively, where $\varphi_{odd} = 1, 3, 5, \ldots N_\varphi - 1$, and $\varphi_{even} = 2, 4, 6, \ldots N_\varphi$. Thus, S_{odd} can be considered original illumination and S_{even} is the 'offset' illumination. Finally, rotation subtraction is implemented by simply calculating the difference between the two matrices.

$$\mathrm{S}_{\mathrm{skin\_removed}}(f, Rx, \varphi_{odd}) = \mathrm{S}_{\mathrm{odd}}(f, Rx, \varphi_{odd}) - \mathrm{S}_{\mathrm{even}}(f, Rx, \varphi_{even}) \ldots\ldots\ldots \quad (1)$$

The signals are converted to the time domain using the Inverse Fourier Transform to generate $\Gamma(t, Rx, \varphi_{odd})$. Subsequently, the data in the $\Gamma(t, Rx, \varphi_{odd})$ was processed using the Coherence Factor Delay-and-Sum (CF-DAS) algorithm [38] for the clear reconstruction of the image [39].

A. SYNTHETIC FOCUSING TECHNIQUES

Normally, DAS based methods excel in such situations as reflections off only one target have to be considered. The presence of multiple targets can cause multiple internal reflections to misguide the imaging system. DMAS achieves the best performance compared to other DAS variants presented in [6] and [40], however it requires significantly longer computation time. Most DAS variants' execution times are linearly dependent on the number of signals in the system. However, DMAS has a quadratic relationship with the number of signals as it generates extra signals by multiplying individual pairs of signals. While this improves the performance, the large computational expense required for a high number of signals becomes a challenge. Furthermore, an iterative approach requires multiple executions of the same algorithm, which compounds the execution time even more. Thus, CF-DAS is utilized in the proposed system as it rewards higher coherence by the Coherence Factor calculated using. This quantity is used to scale the results obtained from conventional DAS. Mapping multiple different targets is usually not attempted or presented in most literature, as it is often difficult for DAS based techniques, which were developed mostly as single target detection methods.

B. DAS

Here ω is angular velocity, and k is the total number of time samples in the scan window. The three-dimensional Cartesian coordinates of each point in the imaging domain are represented in the i by 3 matrices, C, where i is the total number of points. Then the i by i matrix, P_{C-C}, which contains the Euclidian distances between each possible pair of points in the imaging domain, is generated from C. Matrices A_{Tx} and A_{Rx} contain the three-dimensional Cartesian coordinates of the transmitting and receiving antennas, respectively. Since there are 64 distinct channels in a given rotational orientation, and N/2 (N is 50 in this study) orientations are produced, after the rotation subtraction, to be focussed synthetically. Furthermore, as the imaging domain is stationary, the rotating antennas change their distance from the points to be reconstructed. Thus, $A_{Tx\varphi odd}$ and $A_{Rx\varphi odd}$ are generated by determining all the antenna positions considered in the original orientation. Then, $P_{Tx\varphi odd-C}$ and $P_{C-Rx\varphi odd}$, containing the distances from each point to the transmitting and receiving antennas are evaluated from C, $A_{Tx\varphi odd}$, and $A_{Rx\varphi odd}$. Then, the delays required for focusing each channel on a given point in C is calculated by adding the distances of the transmitting and receiving antenna positions concerned to the point being focused. Then, the speed of light in the background medium, which is air in this study, is then divided by the total distance to yield the appropriate delay, $\tau(i, Rx, \varphi_{odd})$.

$$\tau(i, rx, \varphi_{odd}) = \frac{\sqrt{\varepsilon_b}(P_{Tx\varphi_{odd}-C}(i, tx, l) + p_{C-Rx\varphi_{odd}}(i, rx, l))}{c} \quad (2)$$

where ε_b is the dielectric constant of the background medium. The delay is derived from the estimated shortest distance a reflected signal from $C(i)$. This approach does not consider the presence of multiple reflections or the additional propagation delay caused by more dense tissue inside the phantom. After that, the delays are applied to the signals to produce the delayed. The scattering intensity map, $\Upsilon_{DAS}(i)$, is determined by calculating the correlation between the delayed signals. In conventional DAS, the correlation is calculated as follows:

$$\Upsilon_{DAS}(i) = (\int_{-\infty}^{\infty} \sum_{\forall \varphi_{odd}} \sum_{\forall rx} \Gamma \times (t - \frac{\tau(i, rx, \varphi_{odd})}{\Delta t}, rx, \varphi_{odd})dt)^2 \quad (3)$$

where Δt is the time step.

Since DAS simply relies on the coherent summation of delayed signals, it often suffers from the artifacts generated by multiple reflections, especially in nearfield applications. Thus, several approaches have been suggested in the past few decades to improve the conventional DAS algorithm. Improved Delay and Sum, or IDAS, associates a coherence factor based on the energy collection curve [41]. In this study, CF-DAS is utilized to calculate the Υ_0. CF-DAS and IDAS have shown comparable performance in [42].

However, CF-DAS is simpler to implement, as it does not involve relatively more complex operations like those that curve fitting used in IDAS. Delay-Multiply-and-Sum shows superior performance to both CF-DAS and IDAS but requires significantly longer to execute as it has quadratic time complexity concerning the number of channels, whereas, DAS and the other variants exhibit linear time complexity.

C. CF-DAS

CF-DAS implements a weighted sum of the channels. The Coherence Factor is designed to reward more coherent channels at each point in the imaging domain with higher weights. It is calculated as the following:

$$CF(i) = \frac{\Upsilon_{DAS}(i)}{\int_{-\infty}^{\infty} \sum \forall_{\varphi_{odd}} \sum \forall_{rx} \Gamma\left(t - \frac{\tau(i,rx,\varphi_{odd})}{\Delta t}, rx, \varphi_{odd}\right)^2 dt} \tag{4}$$

After that, the scattering intensity map is calculated by the following equation:

$$\Upsilon_{CF-DAS}(i) = CF(i).\Upsilon_{DAS}(i) \tag{5}$$

D. DELAY CALCULATION CORRECTION

Since a higher value of Υ in a region of C can be inferred as a region with higher dielectric constant, time delay caused should be higher as dielectric material reduces the propagation speed. The extra time can be adjusted by appropriately increasing the distances considered in τ calculations. Since modifications to τ translate to an improved estimate of the scattering intensity map, an iterative approach is adapted to determine the best delay and scattering intensity map estimation achievable. However, using Υ directly can cause the iterative process to become unstable and sensitive to noise levels. Thus, a distance inverse weighted integral averaging is applied to produce a smoothed scattering intensity map, Υ *'(i).* The distance inverse weighting is used to reflect the three-dimensional Green function for electromagnetic waves.

$$\Upsilon'(i) = \int_C \frac{\Upsilon^{n-1}_{CF-DAS}(i)}{1 + p_{C-C}(i,j)} dj \tag{6}$$

Then, the modified delay is calculated by the following equation:

$$\tau'(i, rx, \varphi_{odd}) = \tau(i, rx, \varphi_{odd}) + \frac{\Upsilon'(i)}{c} \tag{7}$$

$$\Upsilon^n_{DAS}(i) = \int_{-\infty}^{\infty} \sum \forall_l \sum \forall_{rx} S(rx, \varphi_l, t_k - \frac{\tau'(i, rx, l)}{\Delta t}) dt \tag{8}$$

Then, the coherence factor is calculated, and the CF-DAS scattering intensity map is evaluated as follows:

$$\Upsilon^n_{CF-DAS}(i) = CF(i).\Upsilon^n_{DAS}(i) \tag{9}$$

Based on the new set of delays, the scattering intensity map is reconstructed. Finally, the termination criterion checks for convergence. Equations 6-10 are iteratively evaluated for n = 1, 2 . . . .7.

$$E_\Upsilon = \sum \forall_i \left| \Upsilon^n_{CF-DAS} - \Upsilon^{n-1}_{CF-DAS} \right| \tag{10}$$

The iterative process is prematurely terminated when E_Υ reduces to the desired level of accuracy as convergence has already been achieved. In this study, $E_\Upsilon < 10^{-5}$ is used.

VI. IMAGING RESULTS ANALYSIS AND DISCUSSIONS

The signal to mean ratio (SMR) for the DAS and CDAS image reconstructions is compared to the delay corrected CDAS images in Table 1 below. The SMR is significantly improved in all four phantoms considered which is calculated by averaging the values of Υ across the volume of tumor in the phantoms and determining its ratio to the overall average of Υ in the entire reconstructed volume. The tumor regions are indicated in Figure 9 using red circles. The left side images show results from CF-DAS and the images on the right show the delay corrected CF-DAS results. The images of the developed breast phantoms with identified tumor are shown in Figure 9. The skin reflections are nearly identical for almost every observation as we use cylindrically symmetric homogeneous anatomical phantom (apart from the tumors) and it is placed at the rotation center. A dotted red circle is drawn on the final imaging results to indicate the phantom surface. Figure 9(a) is mostly blank as expected due to the homogeneity of phantom A. Few small insignificant specs of noise appear at the surface of phantom A possibly due to cracks on its exterior.

TABLE 1. Signal to mean ratio, in dB, for phantoms B, C, D, and E.

Phantom	Algorithm		
	DAS	CDAS	CDAS with Delay Correction
Phantom B	7.036	7.8220	18.3132
Phantom C	5.698	15.7206	35.0092
Phantom D	14.334	22.4317	33.4286
Phantom E	4.202	12.3940	31.2602

Furthermore, the iterative correction technique converged after only two iterations as the overall values of Υ were low, which resulted in only minor variation in the delay. Thus, the iterated images barely varied resulting in near identical result CF-DAS on the left and the iteratively enhanced CF-DAS on the right. Figure 9(b) a point of high contrast to the fat material along with some lower intensity clutter for CF-DAS on the left. Note that the highest contrast is produced outside the region of the tumor object. The image on the right

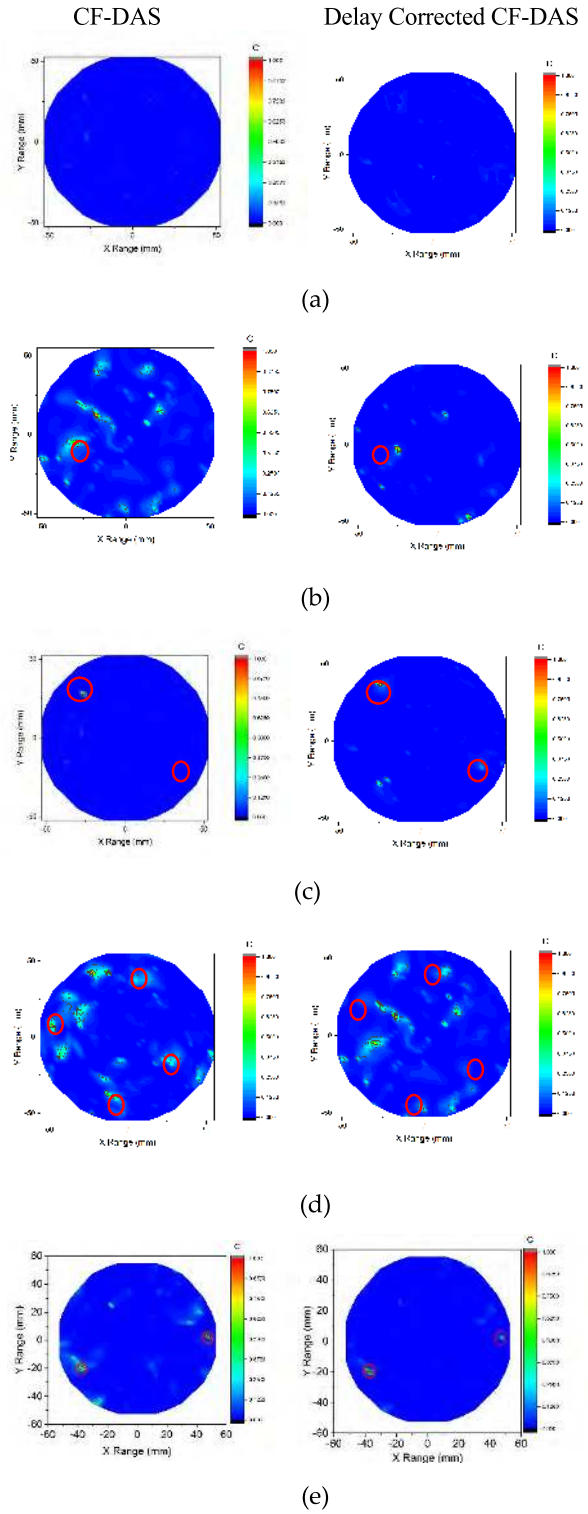

FIGURE 9. Imaging results of homogeneous phantoms (a) without tumor (Phantom A) (b) with a single tumor (Phantom B), (c) with two tumors (Phantom C) d) with four tumors (Phantom D) and e) heterogeneous with two tumor(Phantom E).

clearly shows the noise suppression achieved by the iterative technique while enhancing the tumor response. Figure 9(c) shows two separate clutters indicating the presence of two tumors on the right. Normal CF-DAS did not detect the second tumor object at all. Figure 9(d) shows 'ghosting' around all the tumor potentially due to multiple reflections from the tumor for normal CF-DAS. However, the presence of four distinct clutters indicates the detection of all four tumors on both right and left side. Lastly, the imaging results of the more realistic heterogeneous phantom E with two tumors in Figure 9(e) also shows a significant reduction in clutter by the delay corrected variant. The iteratively enhanced image is significantly clearer than the left side in terms of ghosting. The overall results show marked improvements for tumor object detection in all cases using the iterative approach, which is highlighted further in Table 1.

TABLE 2. Eϒ at each iteration for phantoms B, C, D and E.

Iteration	Phantom B	Phantom C	Phantom D	Phantom E
1	0.46263	0.30259	31.722	1.0585
2	0.005819	0.000807	1.5031	0.006854
3	4.19×10^{-5}	2.00×10^{-6}	0.10818	1.0979×10^{-4}
4	3.15×10^{-7}	$>10^{-7}$	0.012976	1.644×10^{-6}
5	$>10^{-7}$	-	0.001578	$>10^{-7}$
6	-	-	1.910×10^{-4}	-
7	-	-	2.32×10^{-5}	-

Table 2 shows that the proposed iterative method converged for all the phantoms. The error factor exponentially diminished with each iteration. Phantoms B, C, and E converged after 5, 4 and five iterations respectively. Phantom D did not reach the convergence limit of 10^{-7}; however, by extrapolating the results it can conclude that one or two more iterations would have achieved the threshold. The computation is prematurely terminated at seven iterations due to limited execution time. Overall, the proposed algorithm exhibits stable convergence in all cases tested.

VII. CONCLUSION

A microwave system for breast tumor imaging is presented in this article using iteratively corrected coherence factor delay and sum (CF-DAS) algorithm. The proposed modification illustrates a novel technique to improve the performance of data independent radar-based image reconstruction algorithm and convert them to a superior stable data adaptive method with consistent results. The designed imaging system comprises an array of nine improved modified antipodal Vivaldi antennas that can work across the UWB band (2.5 to 11 GHz). A suitable SP8T device is used to enable the eight receiver antennas to 50 rotated position to send reflected microwave signals whereas the reflected backscattered signals are recorded by VNA using the MATLAB based software architecture. Lab-based breast phantom that emulates the dielectric properties of real breast tissues with tumor tissue is fabricated and measured to test the validity of the imaging

system. After collecting the data, an iteratively enhanced CF-DAS algorithm is used to detect the tumors inside the phantoms. Significant improvement on the SMR is observed with the delay correction over both conventional CF-DAS and DAS, making this approach potentially viable for use with other radar-based imaging algorithms.

REFERENCES

[1] C. E. DeSantis, S. A. Fedewa, A. Goding Sauer, J. L. Kramer, R. A. Smith, and A. Jemal, "Breast cancer statistics, 2015: Convergence of incidence rates between black and white women," *CA Cancer J. Clin.*, vol. 66, no. 1, pp. 31–42, 2016.

[2] D. O'Loughlin, M. J. O'Halloran, B. M. Moloney, M. Glavin, E. Jones, and M. A. Elahi, "Microwave breast imaging: Clinical advances and remaining challenges," *IEEE Trans. Biomed. Eng.*, vol. 65, no. 11, pp. 2580–2590, Nov. 2018.

[3] M. Z. Mahmud, M. T. Islam, N. Misran, S. Kibria, and M. Samsuzzaman, "Microwave imaging for breast tumor detection using uniplanar AMC based CPW-fed microstrip antenna," *IEEE Access*, vol. 6, pp. 44763–44775, 2018.

[4] N. K. Nikolova, *Introduction to Microwave Imaging*. Cambridge, U.K.: Cambridge Univ. Press, 2017.

[5] N. Nikolova, *Wiley Encyclopedia of Electrical and Electronics Engineering*. Hoboken, NJ, USA: Wiley, 2014.

[6] W. Shao, A. Edalati, T. R. McCollough, and W. J. McCollough, "A time-domain measurement system for UWB microwave imaging," *IEEE Trans. Microw. Theory Techn.*, vol. 66, no. 5, pp. 2265–2275, May 2018.

[7] M. Abbak, M. N. Akinci, M. Çayören, and I. Akduman, "Experimental microwave imaging with a novel corrugated Vivaldi antenna," *IEEE Trans. Antennas Propag.*, vol. 65, no. 6, pp. 3302–3307, Jun. 2017.

[8] S. M. Salvador, E. C. Fear, M. Okoniewski, and J. R. Matyas, "Exploring joint tissues with microwave imaging," *IEEE Trans. Microw. Theory Techn.*, vol. 58, no. 8, pp. 2307–2313, Aug. 2010.

[9] B. J. Mohammed, A. M. Abbosh, S. Mustafa, and D. Ireland, "Microwave system for head imaging," *IEEE Trans. Instrum. Meas.*, vol. 63, no. 1, pp. 117–123, Jan. 2014.

[10] M. Islam, M. Samsuzzaman, M. Islam, S. Kibria, and M. Singh, "A homogeneous breast phantom measurement system with an improved modified microwave imaging antenna sensor," *Sensors*, vol. 18, no. 9, p. 2962, 2018.

[11] E. Porter, H. Bahrami, A. Santorelli, B. Gosselin, L. A. Rusch, and M. Popović, "A wearable microwave antenna array for time-domain breast tumor screening," *IEEE Trans. Med. Imag.*, vol. 35, no. 6, pp. 1501–1509, Jun. 2016.

[12] M. M. Islam, M. T. Islam, M. R. I. Faruque, M. Samsuzzaman, N. Misran, and H. Arshad, "Microwave imaging sensor using compact metamaterial UWB antenna with a high correlation factor," *Materials*, vol. 8, no. 8, pp. 4631–4651, 2015.

[13] M. Islam, M. Samsuzzaman, M. Islam, and S. Kibria, "Experimental breast phantom imaging with metamaterial-inspired nine-antenna sensor array," *Sensors*, vol. 18, no. 12, p. 4427, 2018.

[14] F. Foroutan and N. Nikolova, "Active sensor for microwave tissue imaging with bias-switched arrays," *Sensors*, vol. 18, no. 5, p. 1447, 2018.

[15] H. M. Jafari, J. M. Deen, S. Hranilovic, and N. K. Nikolova, "Co-polarised and cross-polarised antenna arrays for breast, cancer detection," *IET Microw., Antennas Propag.*, vol. 1, no. 5, pp. 1055–1058, Oct. 2007.

[16] E. Porter, E. Kirshin, A. Santorelli, M. Coates, and M. Popović, "Time-domain multistatic radar system for microwave breast screening," *IEEE Antennas Wireless Propag. Lett.*, vol. 12, pp. 229–232, 2013.

[17] M. Moosazadeh, "High-gain antipodal vivaldi antenna surrounded by dielectric for wideband applications," *IEEE Trans. Antennas Propag.*, vol. 66, no. 8, pp. 4349–4352, Aug. 2018.

[18] X. Li, E. J. Bond, B. D. V. Veen, and S. C. Hagness, "An overview of ultra-wideband microwave imaging via space-time beamforming for early-stage breast-cancer detection," *IEEE Antennas Propag. Mag.*, vol. 47, no. 1, pp. 19–34, Feb. 2005.

[19] W. Shao and R. S. Adams, "Multi-polarized microwave power imaging algorithm for early breast cancer detection," *Prog. Electromagn. Rev.*, vol. 23, pp. 93–107, Mar. 2012.

[20] J.-F. Deprez, M. Sarafianou, M. Klemm, I. J. Craddock, and P. J. Probert-Smith, "Microwave contrast imaging of breast tissue from local velocity estimation," *Prog. Electromagn. Rev.*, vol. 42, pp. 381–403, Sep. 2012.

[21] E. Porter, A. Santorelli, R. Kazemi, and M. Popović, "Microwave time-domain radar: Healthy tissue variations over the menstrual cycle," *IEEE Antennas Wireless Propag. Lett.*, vol. 14, pp. 1310–1313, 2015.

[22] E. Porter, M. Coates, and M. Popović, "An early clinical study of time-domain microwave radar for breast health monitoring," *IEEE Trans. Biomed. Eng.*, vol. 63, no. 3, pp. 530–539, Mar. 2016.

[23] S. Kwon and S. Lee, "Instantaneous microwave imaging with time-domain measurements for breast cancer detection," *Electron. Lett.*, vol. 49, no. 10, pp. 639–641, 2013.

[24] X. Zeng, A. Fhager, M. Persson, P. Linner, and H. Zirath, "Accuracy evaluation of ultrawideband time domain systems for microwave imaging," *IEEE Trans. Antennas Propag.*, vol. 59, no. 11, pp. 4279–4285, Nov. 2011.

[25] X. Zeng, A. Fhager, Z. He, M. Persson, P. Linner, and H. Zirath, "Development of a time domain microwave system for medical diagnostics," *IEEE Trans. Instrum. Meas.*, vol. 63, no. 12, pp. 2931–2939, Dec. 2014.

[26] J. De Zaeytijd, A. Franchois, C. Eyraud, and J.-M. Geffrin, "Full-wave three-dimensional microwave imaging with a regularized Gauss–Newton method—Theory and experiment," *IEEE Trans. Antennas Propag.*, vol. 55, no. 11, pp. 3279–3292, Nov. 2007.

[27] J.-M. Geffrin, P. Sabouroux, and C. Eyraud, "Free space experimental scattering database continuation: Experimental set-up and measurement precision," *Inverse Problems*, vol. 21, no. 6, p. S117, 2005.

[28] C. Eyraud, J.-M. Geffrin, and A. Litman, "3D-aggregate quantitative imaging: Experimental results and polarization effects," *IEEE Trans. Antennas Propag.*, vol. 59, no. 4, pp. 1237–1244, Apr. 2011.

[29] T. Sugitani, S. Kubota, A. Toya, and T. Kikkawa, "A compact 4×4 planar UWB antenna array for 3-D breast cancer detection," *IEEE Antennas Wireless Propag. Lett.*, vol. 12, pp. 733–736, 2013.

[30] H. Song *et al.*, "Detectability of breast tumor by a hand-held impulse-radar detector: Performance evaluation and pilot clinical study," *Sci. Rep.*, vol. 7, Nov. 2017, Art. no. 16353.

[31] T. M. Habashy, R. W. Groom, and B. R. Spies, "Beyond the born and Rytov approximations: A nonlinear approach to electromagnetic scattering," *J. Geophys. Res., Solid Earth*, vol. 98, no. B2, pp. 1759–1775, 1993.

[32] M. N. Akıncı *et al.*, "Qualitative microwave imaging with scattering parameters measurements," *IEEE Trans. Microw. Theory Techn.*, vol. 63, no. 9, pp. 2730–2740, Sep. 2015.

[33] F. Gao, B. D. van Veen, and S. C. Hagness, "Sensitivity of the distorted born iterative method to the initial guess in microwave breast imaging," *IEEE Trans. Antennas Propag.*, vol. 63, no. 8, pp. 3540–3547, Aug. 2015.

[34] Z. Miao and P. Kosmas, "Multiple-frequency DBIM-TwIST algorithm for microwave breast imaging," *IEEE Trans. Antennas Propag.*, vol. 65, no. 5, pp. 2507–2516, May 2017.

[35] M. Abbak, M. Cayoren, and I. Akduman, "Microwave breast phantom measurements with a cavity-backed Vivaldi antenna," *IET Microw., Antennas Propag.*, vol. 8, no. 13, pp. 1127–1133, Oct. 2014.

[36] M. T. Islam, M. Samsuzzaman, S. Kibria, and M. T. Islam, "Experimental breast phantoms for estimation of breast tumor using microwave imaging systems," *IEEE Access*, vol. 6, pp. 78587–78597, 2018.

[37] M. Klemm, I. Craddock, J. Leendertz, A. Preece, and R. Benjamin, "Improved delay-and-sum beamforming algorithm for breast cancer detection," *Int. J. Antennas Propag.*, vol. 2008, Apr. 2008, Art. no. 761402.

[38] M. Klemm, J. A. Leendertz, D. Gibbins, I. J. Craddock, A. Preece, and R. Benjamin, "Microwave radar-based breast cancer detection: Imaging in inhomogeneous breast phantoms," *IEEE Antennas Wireless Propag. Lett.*, vol. 8, pp. 1349–1352, 2009.

[39] H. Bahramiabarghouei, E. Porter, A. Santorelli, B. Gosselin, M. Popović, and L. A. Rusch, "Flexible 16 antenna array for microwave breast cancer detection," *IEEE Trans. Biomed. Eng.*, vol. 62, no. 10, pp. 2516–2525, Oct. 2015.

[40] H. B. Lim, N. T. T. Nhung, E.-P. Li, and N. D. Thang, "Confocal microwave imaging for breast cancer detection: Delay-multiply-and-sum image reconstruction algorithm," *IEEE Trans. Biomed. Eng.*, vol. 55, no. 6, pp. 1697–1704, Jun. 2008.

[41] D. Byrne, M. O'Halloran, M. Glavin, and E. Jones, "Data independent radar beamforming algorithms for breast cancer detection," *Prog. Electromagn. Res.*, vol. 107, pp. 331–348, Jun. 2010.

[42] M. A. Elahi *et al.*, "Comparison of radar-based microwave imaging algorithms applied to experimental breast phantoms," in *Proc. 32nd Internal Union Radio Sci. Gen. Assem. Sci. Symp. (URSI GASS)*, Aug. 2017, pp. 1–4.

SALEHIN KIBRIA was born in Dhaka, Bangladesh, in 1988. He received the B.Eng. degree (Hons.) in electronics majoring in telecommunications from Universiti Kebangsaan Malaysia (UKM), Malaysia, and the M.Sc. degree (Hons.) in electronics majoring in telecommunications from Multimedia University (MMU). He is currently pursuing the Ph.D. degree with UKM. He is a Research Assistant with the Faculty of Engineering and Built Environment (FKAB), UKM, where he is involved in a research project funded by Malaysian Government. His research interests include microwave imaging, RFID systems, and heuristic optimization techniques.

MD SAMSUZZAMAN was born in Jhenaidah, Bangladesh, in 1982. He received the B.Sc. and M.Sc. degrees in computer science and engineering from Islamic University, Kushtia, Bangladesh, in 2005 and 2007, respectively, and the Ph.D. degree from Universiti Kebangsaan Malaysia, Malaysia, in 2015. From 2008 to 2011, he was a Lecturer with Patuakhali Science and Technology University (PSTU), Bangladesh, where he was an Assistant Professor, from 2011 to 2015. He is currently an Associate Professor with PSTU. He is a Postdoctoral Fellow with Universiti Kebangsaan Malaysia. He has authored or co-authored about 80 research journal articles, nearly 20 conference articles, and a few book chapters on various topics related to antennas, microwaves, and electromagnetic radiation analysis. He holds one inventory filed patents. His Google scholar citation is 546 and *h*-index is 13. His research interests include the communication antenna design, satellite antennas, and microwave imaging.

MD TARIKUL ISLAM was born in Patuakhali, Bangladesh, in 1994. He received the B.Sc. degree in computer science and engineering from Patuakhali Science and Technology University (PSTU), in 2016. He is currently pursuing the master's degree with Universiti Kebangsaan Malaysia (UKM), Malaysia. He is currently a Graduate Research Assistant with the Department of Electrical, Electronic and Systems Engineering, UKM. He has authored or co-authored a number referred journals and conference papers. His research interests include the communication antenna design, wireless communication, and RF engineering and microwave imaging.

MD ZULFIKER MAHMUD received the B.Sc. and M.Sc. degrees in computer science and engineering from Islamic University, Kushtia, Bangladesh, and the Ph.D. degree from Universiti Kebangsaan Malaysia (UKM), Malaysia. He is currently an Assistant Professor with the AIS Department, Jagannath University, Bangladesh. He is a Graduate Research Assistant with the Department of Electrical, Electronic and Systems Engineering, UKM. He has authored or co-authored a number referred journals and conference papers. His research interests include the microwave imaging, antenna design, satellite antennas, satellite communication, and wireless communication.

NORBAHIAH MISRAN received the B.Eng. degree in electrical, electronic, and system engineering from Universiti Kebangsaan Malaysia, UKM, in 1999, and the Ph.D. degree from the Queen's University of Belfast, U.K., in 2004. She started her career as a Tutor, in 1999. She was appointed as a Lecturer, in 2004, and an Associate Professor, in 2009. She is currently a Professor with UKM. She has authored or co-authored about 200 research journal articles and nearly 100 conference articles. Her research interests include RF device design particularly in broadband microstrip antennas, reconfigurable antennas, and reflect array antennas. She is also conducting some researches in engineering education field.

MOHAMMAD TARIQUL ISLAM is currently a Professor with the Department of Electrical, Electronic and Systems Engineering, Universiti Kebangsaan Malaysia, and a Visiting Professor with the Kyushu Institute of Technology, Japan. He has authored or co-authored about 350 research journal articles, nearly 165 conference articles, and a few book chapters on various topics related to antennas, microwaves, and electromagnetic radiation analysis. He holds 16 inventory filed patents. His publications have been cited 4210 times, and his *h*-index is 33 (Source: Scopus). His Google scholar citation is 5545 and *h*-index is 36. His research interests include communication antenna design, radio astronomy antennas, satellite antennas, and electromagnetic radiation analysis. He is a Chartered Professional Engineer (CEng) and a member of IET, U.K., and IEICE, Japan. He received more than 40 research grants from the Malaysian Ministry of Science, Technology and Innovation, Ministry of Education, the UKM Research Grant, international research grants from Japan and Saudi Arabia, the Special Award from Vietnam for his research and innovation, the Best Researcher Award from UKM, in 2010 and 2011, the Publication Award from Malaysian Space Agency, in 2009, 2010, 2013, and 2014, and the Best Paper Presentation Award at the 2012 International Symposium on Antennas and Propagation (ISAP 2012), Nagoya, Japan, and at 2015 IconSpace. He was a recipient of several international gold medal awards and the Best Invention in Telecommunication Award. He also received the Best Innovation Award, in 2011, and the Best Research Group in ICT niche, in 2014, from UKM. He currently serves as the Editor-in-Chief for the *International Journal of Electronics, Informatics* and an Associate Editor for *Electronics Letters*.